Nanoscale

Accepted Manuscript

This article can be cited before page numbers have been issued, to do this please use: Q. Zhang, J. Luo, Y. Wang, W. Yan, M. Y. Yuan, Y. Jia, Q. Yu, Y. Zou, X. Zhai and H. Yang, *Nanoscale*, 2025, DOI: 10.1039/D5NR01098E.

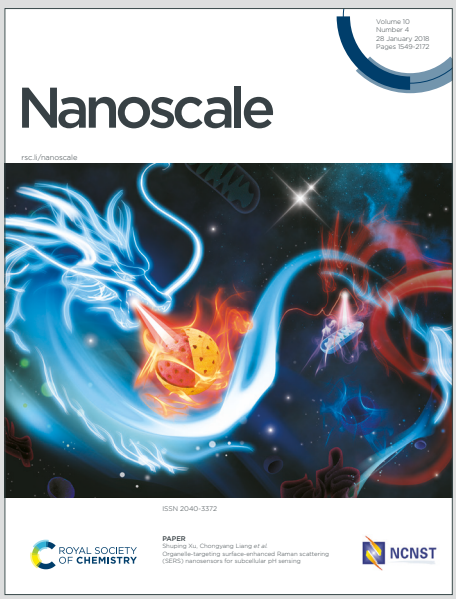

ROYAL SOCIETY OF CHEMISTRY

rsc.li/nanoscale

View Article Online
DOI: 10.1039/D5NR01098E

ARTICLE

Efficient and sustainable preparation of fine particles by bubble-assisted freeze-dissolving method

Received 00th January 20xx,
Accepted 00th January 20xx

DOI: 10.1039/x0xx00000x

Qiutong Zhang[†], Jiaqi Luo[†], Yingchen Wang[†], Wenhao Yan[†], Mingting Yuan[†], Yimin Jia[†], Qiushuo Yu[†], Xinyue Zhai[†], Yuan Zou[†], Huaiyu Yang[*‡]*

The development of fine particles has enabled innovative solutions across energy, environmental, and biomedical applications, driving the demand for cleaner, more efficient, and environmentally friendly synthesis methods. In this study, we present a freeze-dissolving approach as a sustainable and energy-efficient alternative to conventional freeze-drying for the preparation of fine particles $KHCO_3$ and $NH_4H_2PO_4$ particles. By dripping aqueous solutions of $KHCO_3$ or $NH_4H_2PO_4$ into liquid nitrogen, ice-templated particles were rapidly formed and these ice particles were subsequently dissolved in ethanol below 273.15 K. As the ice quickly dissolved in ethanol, the fine particles formed within the ice templates were released into the solution and collected for characterization, including size distribution analysis, SEM imaging, and powder XRD. Compared with freeze-drying, the freeze-dissolving method yields significantly smaller particles while reducing energy consumption by 99%. Moreover, the first-time introduction of air bubbles during the freezing dissolving step further reduces particle size and substantially limited the agglomeration. This bubble- assisted freeze-dissolving technique proves more effective than non-bubbled methods across a range of initial solute concentrations and ice particle sizes, highlighting its potential as a scalable and eco-conscious strategy for fine particle production.

Introduction

Fine particles typically possess a large specific surface area, which holds great significance in scientific research and industrial applications [1–3]. As the particle size diminishes, the surface energy of fine particles correspondingly increases [4,5]. This increase not only intensifies the surface-related catalytic [6,7] and adsorption effects [3] but may also alter the electronic structure of the material and the intermolecular interactions [8–10]. Fine particles can be employed in catalytic processes as they offer an extensive surface area to facilitate chemical reactions [11–13]. Furthermore, their high adsorption capability makes them highly valuable in fields such as environmental purification and sensor development. For instance, a study reported the adsorption behavior of superfine powdered activated carbon (SPAC) on typical precursors of nitroso dimethylamine (NDMA), underscoring how reducing particle size significantly enhances adsorption efficiency [14]. Research also investigated the adsorption site accessibility of SPAC incorporated into electro spun polystyrene fibers, revealing that integrating SPAC into fibers is an effective method for applications like water treatment and gas adsorption [15]. An embedded nano spin sensor was developed for in situ detection of gas adsorption within porous organic frameworks [16]. Micro - and nanoscale metal particles may exhibit unique optical or magnetic properties, which could be potentially applied in medical imaging and data storage technologies [17,18]. Moreover, the small size effect and quantum size effect can lead to the physical properties of fine particles, such as electrical properties [19], thermal properties [20], and melting point [21], differing markedly from those of macroscopic materials. This brings new research directions to materials science. These unique properties of fine particles make them play a crucial role in research related to chemical production. Precisely controlling the size, shape and composition of particles enables researchers to design a new generation of functional materials to address current and future technological challenges and meet the demands of increasingly demanding applications.

In agriculture, the high specific surface area and dispersibility of fine particles enhance fertilizer efficiency. Fine particles of $NH_4H_2PO_4$ have been applied and investigated with its fertilizer effect [22]. The smaller $NH_4H_2PO_4$ particles significantly enhance fertilizer efficiency. Fine particles have a higher specific surface area, increasing contact probability with plant roots. This accelerates nutrient release, ensures more uniform distribution, and allows plants

[†] *School of Chemical Engineering, Northwest University; Chemical Engineering Research Center of the Ministry of Education for Advanced Use Technology of Shanbei Energy; International Science & Technology Cooperation Base of MOST for Clean Utilization of Hydrocarbon Resources, Xi'an, Shaanxi 710069, China*
[‡] *Department of Chemical Engineering, Loughborough University, Loughborough LE11 3TU, United Kingdom Department of Chemical Engineering, Loughborough University, Loughborough LE11 3TU, United Kingdom*
[*] *Corresponding authors. E-mail:* H.yang3@lboro.ac.uk

yuqiushuo@nwu.edu.cn
Supporting Information:

View Article Online
DOI: 10.1039/D5NR01088B

to absorb key nutrients like nitrogen and phosphorus more efficiently. In the food industry and animal husbandry, the good dispersibility and flowability of fine particles improve production efficiency and product quality. In fire-extinguishing applications, the small $KHCO_3$ particles from B-FDas show higher efficiency. They quickly cover the fire source and efficiently release fire-extinguishing gases. The smaller $KHCO_3$ particles increase decomposition rates and fire-extinguishing efficiency [23].

The freeze-dissolving in antisolvent method (FDas) [24–26] have been used to produce nano and micro particles. The method involved dropping a solution of $KHCO_3$ into liquid nitrogen to form spherical ice particles. Subsequently, the ice scaffolds were rapidly dissolved in a cryogenically jacketed beaker with magnetic stirring using a dose of antisolvent ethanol corresponding to five to seven times the $KHCO_3$ solution, and the fine particles were recovered by filtering. Many technologies have been utilized to produce fine particles, such as ball milling, chemical precipitation, and sol-gel methods. Ball milling achieves fine particle sizes through mechanical grinding. However, it may introduce impurities and lead to irregular particle shapes [27–29]. Chemical precipitation forms particles via chemical reactions in solution. But it demands strict control of reaction conditions and often results in particles with a broad size distribution [30–32]. The sol-gel method involves transitioning a solution into a gel to create particles, but it is rather complex and time-consuming [33–35]. The FDas method had a quicker dissolving rate, a smaller equipment footprint, and produced fine particles with improved dispersion than conventional freeze-drying (FDry). However, in many conditions, it is still challenging to make particles below 10 μm, and aggregation between particles still needs to be improved.

In this work, we developed a novel method, bubble-assistant freeze-dissolving in antisolvent (B-FDas), which involves the introduction of continuous air bubbles during the freeze-dissolving process. This advanced technique produced smaller fine particles with less agglomerations for both the $KHCO_3$ and $NH_4H_2PO_4$ systems. The study encompassed various initial concentrations ranging from 0.02 g/g to 0.10 g/g and frozen ice particle volumes varying from 0.01 to 0.08 cm^3. The resulting products were characterized using powder XRD, SEM. The size distributions were determined. Furthermore, the mechanisms and effects of air bubbles during the freeze-dissolving process were discussed.

Experimental section

Materials

Potassium bicarbonate ($KHCO_3$) was purchased from Tianjin Baishi Chemical Co., Ltd. (purity > 99.5%). Ethanol was purchased from Tianjin Damao Chemical Reagent Factory (purity > 99.7%). Liquid nitrogen with purity > 99.8% was purchased from Xi'an Aier Industrial Gas Co., Ltd. (China). Ammonium dihydrogen phosphate ($NH_4H_2PO_4$) was purchased from Tianjin Damao Chemical Reagent Factory (purity > 99%). All chemicals were used without further purification. In the whole measurement process, distilled deionized water (conductivity, less than 0.5 μS/cm) prepared in our laboratory was used.

Frozen spherical particles formation

Aqueous solutions of $KHCO_3$ were prepared by dissolving 0.2 g, 0.5 g and 1.0 g of $KHCO_3$ in 10 g of water at 295.15 K. $KHCO_3$ frozen spherical particles with an average volume of 0.04 cm^3 were prepared by dropping these solutions into a holding vessel containing approximately 10 mL of liquid nitrogen using a pipette. The aqueous $KHCO_3$ solution with a concentration of 0.02 g/g was prepared and dropped into liquid nitrogen using different sized pipettes to produce $KHCO_3$ frozen spherical particles with an average volume of 0.06 cm^3 and 0.08 cm^3, respectively. Following the same procedure, aqueous solutions of $NH_4H_2PO_4$ were prepared by dissolving $NH_4H_2PO_4$ in 10 g of water at the same room temperature at concentrations of 0.02 g/g, 0.06 g/g and 0.10 g/g, respectively. Frozen spherical $NH_4H_2PO_4$ particles were produced with an average volume of about 0.04 cm^3. With 0.02 g/g $NH_4H_2PO_4$, 0.01 cm^3 and 0.04 cm^3 frozen ice spherical particles were prepared.

Fine particles production

B-FDas (Bubble-assistant Freeze-dissolving in antisolvent), FDas (Freeze-dissolving in antisolvent) and FDry (Freeze-drying) were applied to obtain particles of $KHCO_3$ and $NH_4H_2PO_4$, as shown in **Figure 1**. The frozen spherical ice particles of $KHCO_3$ or $NH_4H_2PO_4$ were added to the antisolvent ethanol (mass ratio of inorganic aqueous solution to ethanol 1:7) in the jacketed beaker with continues stirring at 400 rpm. The jacketed beaker was put in a cold-water bath at 253.15 K. For B-FDas method, air bubbles with diameter about 900 μm were injected into the solution with the flow rate of 1 L/min. The temperature of air bubbles was room temperature and approximately 295.15 K. After the ice framework was completely dissolved, the particles were collected after filtration. The different sizes of the frozen spherical particles were used following the same procedure. For FDry method, the frozen particles were put in freeze dryer (FD-1A-50, Beijing Biocon Scientific Instrument Co., Ltd.) in freeze temperature and vacuumed condition, till all water molecules sublimation and the particles of $KHCO_3$ and $NH_4H_2PO_4$ were collected.

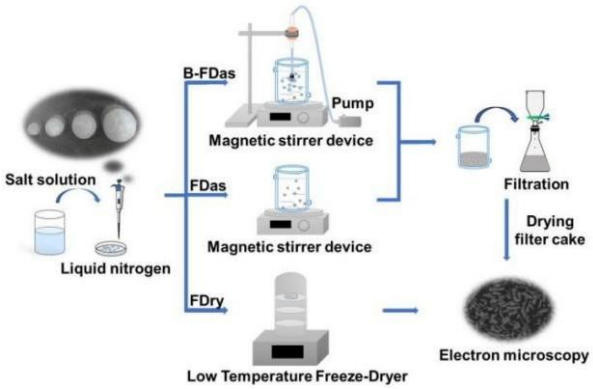

Figure 1. Schematic diagram of the experimental setup and experimental procedure for B-FDas, FDas and FDry.

View Article Online
DOI: 10.1039/D5NR01088E

Air bubbles in dissolving

Frozen spherical particles of $KHCO_3$ at a concentration of 0.08 g/g and a volume of 0.04 cm^3 were prepared into small particles using FDry, and then the particles were divided into three groups, one group was kept sealed as the original sample, and the other two groups were immersed into a mixture of water and ethanol and were operated under stirring with air bubbles and without. The mass ratio of the sample fine particles, water, and ethanol was 0.08:1:7. The mixing time was always controlled to be 30 seconds and the mixing speed to be 400 rpm for both groups to maintain consistency. After this, the products were collected after filtrations.

Characterizations

About 0.5 g product particles were added into 20 mL of ethanol with ultrasonic treatment for 10 minutes. The size distributions of the samples were determined by Master sizer 2000 (Malvern). The measurement of each sample was repeated three times and the data provided in the text below is the equivalent spherical diameter.

The dried product pellets were fixedly placed on the sample stage of the SEM and properly mounted. A scanning electron microscope (TM3000, Hitachi High Technologies Co., Ltd., Japan) was activated to calibrate the relevant parameters to ensure the clarity and accuracy of the images, and the quality and degree of detail of the images were controlled by adjusting the scanning speed and scanning range of the electron microscope. The acquired images were processed and analyzed to obtain clearer and more accurate images.

The product samples were ground, pressed and coated to obtain a flat and homogeneous sample surface. The samples prepared were placed in the sample holder of the XRD instrument and the Smart lab Powder Diffractometer with radiation (1.5406 Å) was activated to determine the powder X-ray diffraction of the product samples.

The crystallinity (X_C) of product samples was evaluated by analysing the XRD patterns using Origin software, following the equation 1.

$$X_C = \frac{A_C}{A_C + A_a} \quad \text{Eq.1}$$

where A_c represents the area of crystalline diffraction peaks in the XRD pattern, and A_a represents the area of amorphous (or non-crystalline) scattering in the XRD pattern.

Results and discussions

Influences of different sizes of frozen spherical particles

As illustrated in **Figure 2**, a comparison of the particle size distributions for fine particles prepared using three different methods reveals that the B-FDas method produces significantly smaller particle size distributions compared to the FDas and FDry methods across all three frozen spherical particle sizes. This trend is consistent for both the $KHCO_3$ and $NH_4H_2PO_4$ systems. The results indicate that the introduction of gas bubbles effectively contributes to reducing particle size.

Table 1 shows the $KHCO_3$ particles obtained by B-FDas method, the B-FDas method consistently produces significantly smaller average particle sizes across all three frozen spherical particle volumes. With frozen particles of 0.04 cm^3, the average size of final products achieved is 10.20 ± 0.63 μm with B-FDas, compared to 24.70 ± 0.55 μm with FDas and 101.40 ± 0.84 μm with FDry. With frozen particle size increased to 0.08 cm^3, B-FDas lead to smaller particle sizes (13.11±0.89 μm) compared with particles obtained with FDas (15.85 ± 0.99 μm) and particles obtained with FDry (103.61±2.41 μm). A similar trend is observed with $NH_4H_2PO_4$ particles, where B-FDas consistently lead to smaller sizes, such as that with frozen particle size increased to 0.04 cm^3, products are 13.67±0.73 μm with B-FDas compared to 20.87 ±0.94 μm with FDas and 25.25±1.07 μm with FDry.

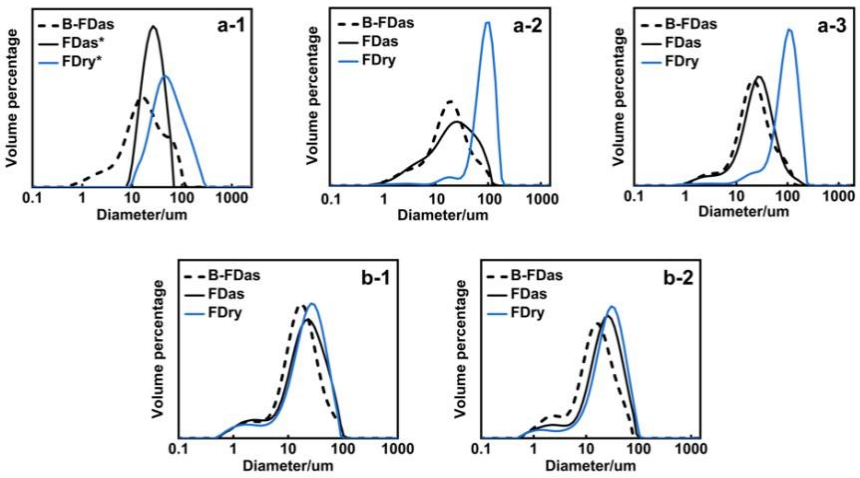

Figure 2. In three methods (B-FDas, FDas[25] and FDry [25].), at the concentration of 0.02 g/g, the particle size distribution of $KHCO_3$ frozen spherical particles having three different average volumes: (a-1) 0.04 cm^3, (a-2) 0.06 cm^3 and (a-3) 0.08 cm^3; the particle size distribution of $NH_4H_2PO_4$ frozen spherical particles having different average volumes: (b-1) 0.01 cm^3, (b-2) 0.04 cm^3.

View Article Online
DOI: 10.1039/D5NR01098E

Table 1. Average particle size of fine particles obtained by B-FDas, FDas and FDry for different sizes of frozen spherical particles.

Frozen ice particle size	0.04 cm^3	0.06 cm^3	0.08 cm^3
$KHCO_3$	Average particle size ± standard deviation (Span)/μm		
B-FDas	10.20±0.63 (2.03)	10.96±0.79 (1.98)	13.11±0.89 (1.90)
FDas	24.70*±0.55 (1.44)	13.25±0.85 (2.17)	15.85±0.99 (1.69)
FDry	101.40*±0.84 (2.79)	93.94±2.56 (1.36)	103.61±2.41 (1.61)
Frozen ice particle size	0.01 cm^3	0.04 cm^3	
$NH_4H_2PO_4$	Average particle size ± standard deviation (Span)/μm		
B-FDas	14.94±0.77 (1.84)	13.67±0.73 (1.95)	
FDas	19.00±0.87 (1.98)	20.87±0.94 (1.80)	
FDry	21.23±0.95 (1.87)	25.25±1.07 (1.88)	

**$KHCO_3$ was obtained using both FDas and FDry methods [25]. For both $KHCO_3$ and $NH_4H_2PO_4$, the concentration at various volumes was maintained at 0.02 g/g. Span=(D90 – D10)/D50.*

Table 1 shows that despite the increase in the volume of $KHCO_3$ frozen ice particle sizes from 0.04 cm^3 to 0.08 cm^3, the average size of fine particles prepared by the B-FDas method remains stable at approximately 10 μm. Nevertheless, it is notable that the average size of fine particles with both the FDas and FDry methods are larger than that with the B-FDas method. In the $KHCO_3$ system, the average particle sizes of the small particles obtained by the FDry method are all approximately 100 μm, which is significantly larger than the particles with the B-FDas method. Fine particles of $KHCO_3$ and $NH_4H_2PO_4$ particles obtained by the B-FDas method have uniform particle size distribution, proved by relatively small Span values under all the conditions. For $KHCO_3$, fine particles with frozen particle volumes of 0.04 cm^3, 0.06 cm^3, and 0.08 cm^3 have the Span values of 2.03, 1.98, and 1.90, respectively. For $NH_4H_2PO_4$, fine particles with frozen particle volumes of 0.01 cm^3 and 0.04 cm^3 have Span values of 1.84 and 1.95, respectively. The fine particles obtained by FDas and FDry method have similar Span value as those obtained by B-FDas, which due to the average size D50 are larger. Comparing with value of D90 – D10, the fine particles by B-FDas are smaller than those obtained by FDas and FDry methods.

Figure 3 and **Figure 4** show the SEM images of $KHCO_3$ and $NH_4H_2PO_4$ fine particles. Particles with B-FDas have less agglomeration. It is noted that the $KHCO_3$ particles obtained by FDas and FDry in this work are consistent with previous reports[25]. **Figure 3** shows that $KHCO_3$ particles by B-FDas method are much smaller particles compared to the other two techniques. The particles produced by B-FDas have a regular morphology with minimal aggregation. In contrast, particles prepared by the FDas and FDry methods exhibit significant aggregation. $KHCO_3$ particles by FDry method shows irregularly shaped particles with extensive aggregation. **Figure 4** shows $NH_4H_2PO_4$ particles by B-FDas method have a more consistent and regular morphology, while the FDas and FDry methods result in larger and heavily aggregated particles.

View Article Online
DOI: 10.1039/D5NR01098E

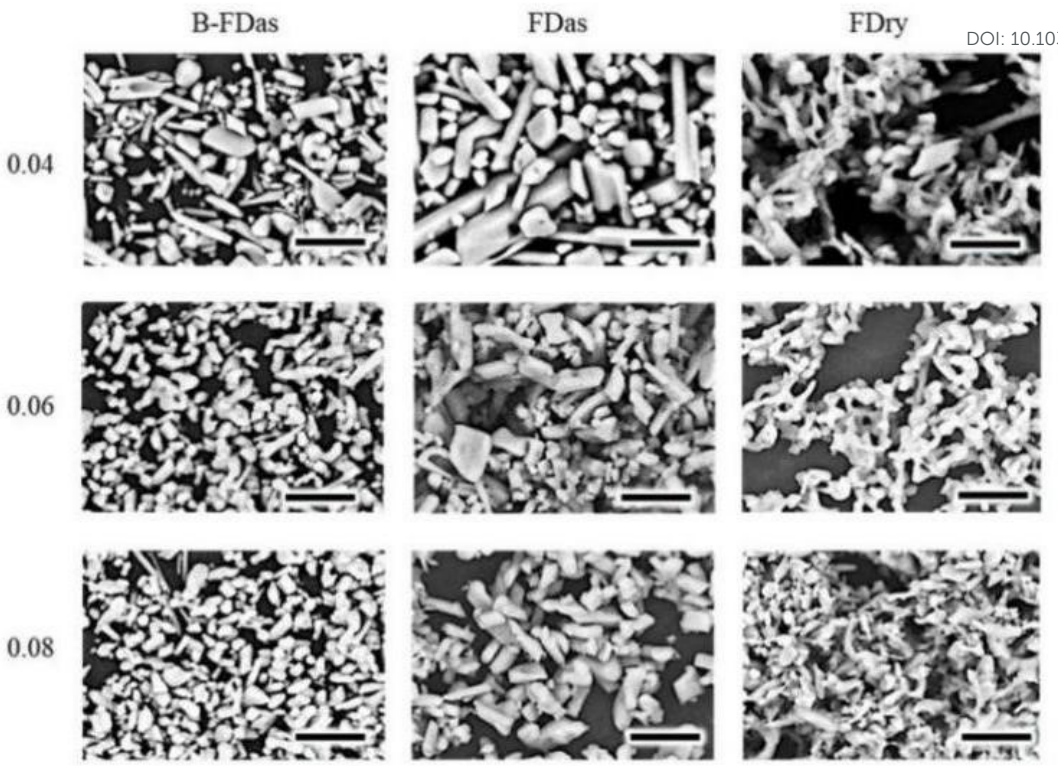

Figure 3. SEM images of $KHCO_3$ crystalline particles by the B-FDas (left), FDas (middle) and FDry (right) obtained from the frozen spherical particles with average size of 0.04 cm^3(top), 0.06 cm^3(middle) and 0.08 cm^3 (bottom). Scale bar: 10 μm.

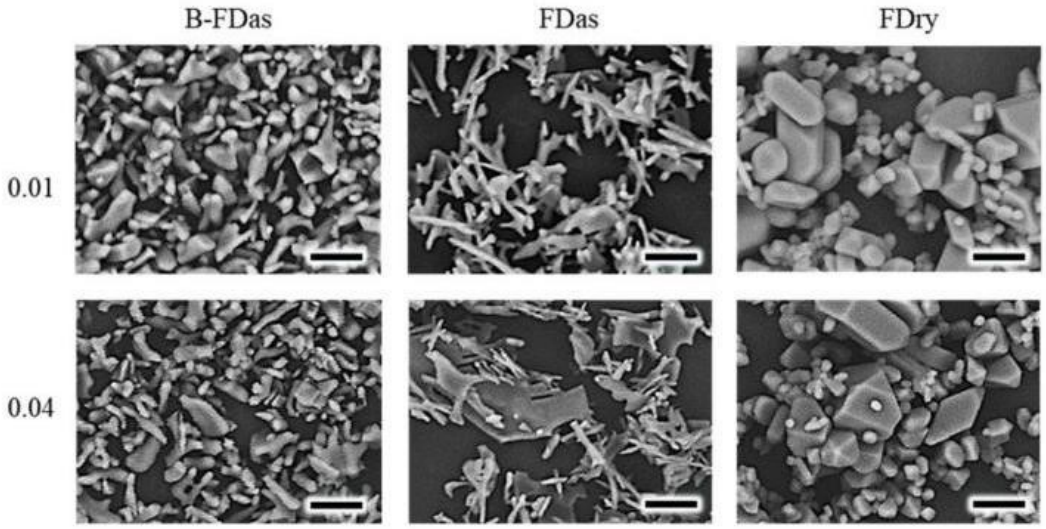

Figure 4. SEM images of $NH_4H_2PO_4$ crystalline particles by the B-FDas (left), FDas (middle) and FDry (right) obtained from the frozen spherical particles with average size of 0.01 cm^3(top) and 0.04 cm^3 (bottom). Scale bar: 10 μm.

The XRD patterns in **Figure 5** show the $KHCO_3$ and $NH_4H_2PO_4$ fine particles maintained have all good crystalline structure, obtained with all three methods, B-FDas, FDas and FDry method, as well as raw materials. We can observe that although three different methods were used to obtain fine particles, their XRD images showed a high degree of consistency. The diffraction peaks of each group of samples can correspond to each other, which shows that the obtained $KHCO_3$ and $NH_4H_2PO_4$ fine particles maintained the same phase in the crystal structure regardless of whether the B-FDas, FDas or FDry method. The crystallinity of the samples based on Equ. 1 for the $KHCO_3$ products prepared by B-FDas, FDas, FDry methods and the raw material were 0.78, 0.77, 0.78, and 0.79, respectively. The crystallinity for $NH_4H_2PO_4$ products prepared by B-FDas, FDas, FDry methods and the raw material were 0.82, 0.81, 0.83, and 0.85, respectively. All products, as well as raw materials, had high crystallinity. These results not only confirm the reliability of the

View Article Online
DOI: 10.1039/D5NR01098E

preparation method, but also demonstrate that the introduction of gas bubbles did not alter the crystal structure of the material.

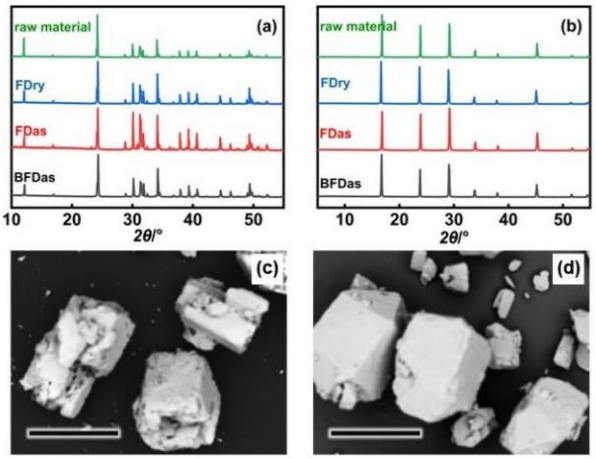

Figure 5. Powder X-ray diffraction patterns (a) $KHCO_3$ and (b) $NH_4H_2PO_4$ of the raw material and the product particles obtained by B-FDas, FDas, and FDry methods. The product particles obtained from the frozen ice particle size of 0.04 cm^3 by the 0.02 g/g solution. SEM images of the raw materials of (c) $KHCO_3$ and (d) $NH_4H_2PO_4$. Scale bar: 1 mm.

Influences of different concentrations of the solution

Figure 6 shows that the products with B-FDas method are smaller all conditions. The particle size increases as the concentration of solution increases. The particles with FDas and FDry are larger , especially at higher concentrations of solution for preparing the frozen particles.

Table 2 shows that particles by B-FDas have the smallest average particle sizes for both $KHCO_3$ and $NH_4H_2PO_4$ systems, ranging from 10.20 ± 0.63 μm to 13.64 ± 0.72 μm for $KHCO_3$, compared to much larger sizes with FDas and FDry, which can reach up to 148.40 ± 1.02 μm. As the concentration of $NH_4H_2PO_4$ solution increases, the particles produced by the B-FDas method become smaller and more uniform, with particle size increasing from 13.67 ± 0.73 μm with the solution of 0.02 g/g concentration to 18.10 ± 0.87 μm with solution of 0.10 g/g concentration. Particles produced by the FDas method show an increase in particle size as the concentration increased, increasing from 20.87 ± 0.94 μm at a concentration of 0.02 g/g to 24.31 ± 0.95 μm at a concentration of 0.10 g/g. Furthermore, particles produced by the FDry method are larger, with a maximum size of 68.27 ± 1.62 μm. Particles produced by the B-FDas method had the more proportion of smaller particles.

Under various concentration conditions, the Span values of the products obtained by B-FDas method remain similar. In the $KHCO_3$ system, when the solution concentration increased from 0.02 g/g to 0.10 g/g, the Span value of the fine products by B-FDas method in the range of 2.03 to 2.24. The Span values of the fine products by FDas method and by FDry method are in range of 1.44 to 1.89, and 2.11 to 2.79, respectively. In the $NH_4H_2PO_4$ system, all the Span values of all fine products are in the range of 1.7 to 2.0, and the average size of the fine products by B-FDas method are smallest, followed by the products by FDas method and FDry methods.

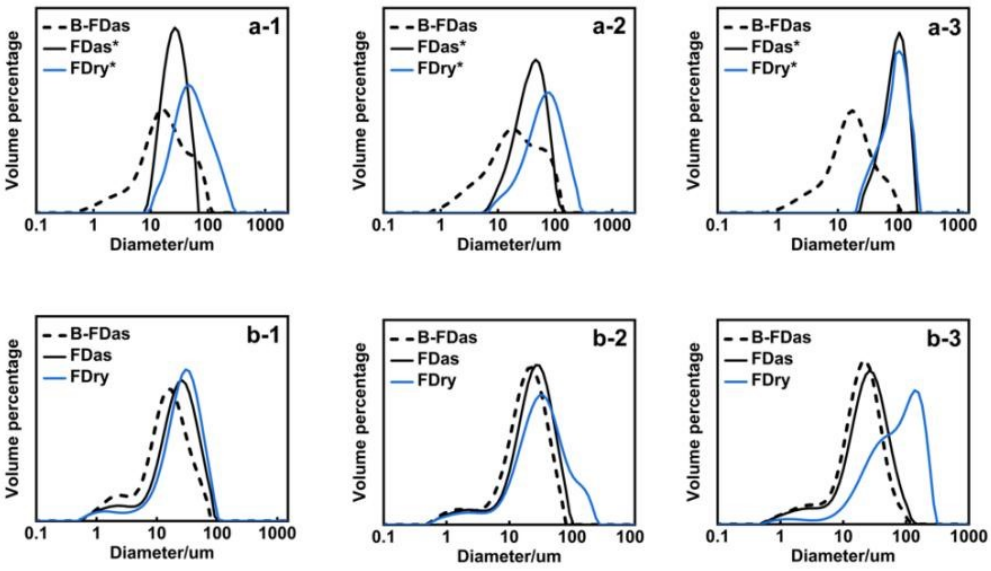

Figure 6. The particle size distribution of $KHCO_3$ fine particles obtained by three methods at four concentrations: (a-1) 0.02 (same as Figure 2 (a-1)), (a-2) 0.05, (a-3) 0.10 g/g; The particle size distribution of $NH_4H_2PO_4$ fine particles obtained by three methods at three concentrations: (b-1) 0.02 (same as Figure 2 (b-1)), (b-2) 0.06, (g) 0.10 g/g. The volumes of the two particles at various concentrations are both 0.04 cm^3. *FDas and FDry of $KHCO_3$ [25].

View Article Online
DOI: 10.1039/D5NR01098E

Table 2. Average particle size of fine particles obtained by B-FDas, FDas and FDry for different concentrations of frozen spherical particles.

Concentration	0.02 g/g	0.05 g/g	0.10 g/g
$KHCO_3$	Average particle size ± standard deviation (Span)/μm		
B-FDas	10.20±0.63 (2.03)	11.21±0.63 (2.19)	13.64±0.72 (2.24)
FDas	24.70*±0.55 (1.44)	55.80*±0.74 (1.89)	143.59*±1.09 (1.77)
FDry	101.40*±0.84 (2.79)	148.40*±1.02 (2.21)	146.20*±1.46 (2.11)
Concentration	0.02 g/g	0.06 g/g	0.10 g/g
$NH_4H_2PO_4$	Average particle size ± standard deviation (Span)/μm		
B-FDas	13.67±0.73 (1.95)	17.69±0.88 (1.75)	18.10±0.87 (1.73)
FDas	20.87±0.94 (1.80)	22.60±0.99 (1.74)	24.31±0.95 (1.81)
FDry	25.25±1.07 (1.88)	28.90±1.00 (1.88)	68.27±1.62 (1.93)

**FDas and FDry of $KHCO_3$ [25]. The volumes of the two particles at various concentrations were both 0.04 cm^3. Span=(D90 – D10)/D50*

Figure 7 and **Figure 8** show that the $KHCO_3$ and $NH_4H_2PO_4$ particles prepared by B-FDas have more regular shapes. In contrast, the particles prepared by FDas have more irregular shapes with heavier agglomeration. This may be due to the presence of air bubbles reduces the contact between particles, thus reducing the possibility of agglomeration. In contrast, particles with FDry are largest with the heaviest agglomeration. Less agglomeration of the particles with B-FDas method could improve the flowability.

The SEM images show the morphology of the fine particles are different for $KHCO_3$ and $NH_4H_2PO_4$ at similar range of supersaturation with same freeze dissolving process, which were determined by the properties of material and compounds. Besides, as the fine particles were formed during the freezing process, the morphology of the particles will be dependent on supersaturation. With higher supersaturation, by faster freezing rate, smaller droplet volume or higher concentration in the droplet solution, the particles tended to be smaller or to be needle-shape. The dissolving process would also influence the morphology, but the effect was much limited than the freezing process. The dissolving process could lead to dissolving some of the very tiny particles, or breakage of the needle crystals by air bubbles inside solution.

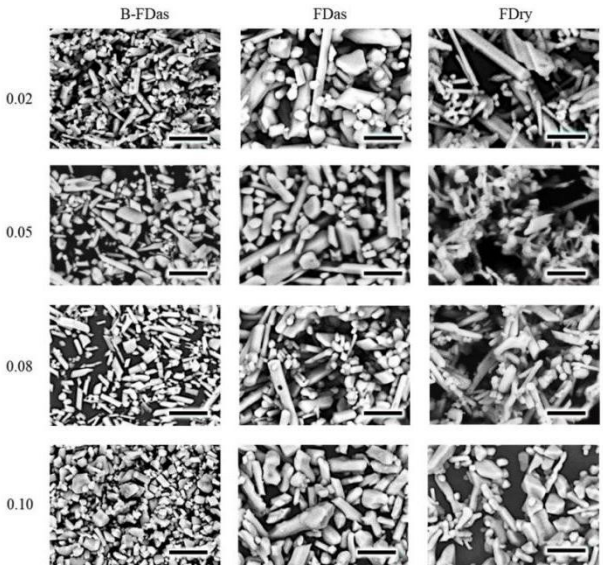

Figure 7. The SEM images of $KHCO_3$ crystalline microparticles prepared with B-FDas (left), FDas (center), and FDry (right) with frozen spherical particles at concentrations of 0.02 g/g (first row), 0.05 g/g (second row), 0.08 g/g (third row), and 0.10 g/g (fourth row), respectively. The volume of the prepared frozen spherical particles was 0.04 cm^3. Scale bar: 10 μm.

View Article Online
DOI: 10.1039/D5NR01098E

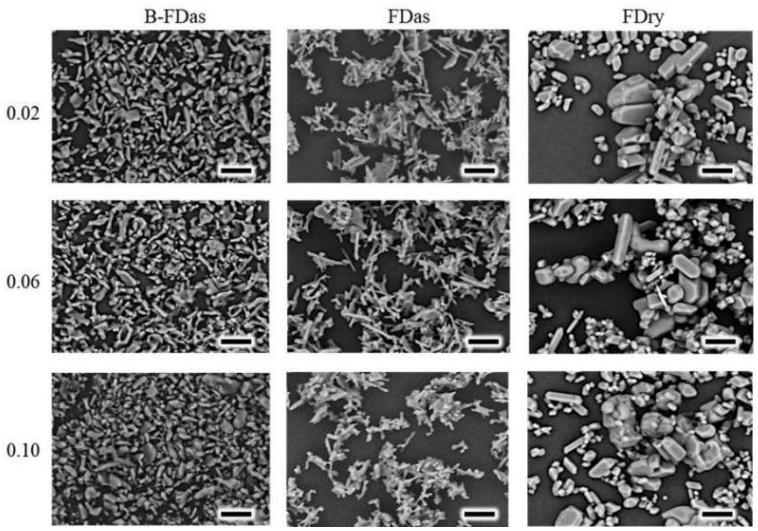

Figure 8. The SEM images of $NH_4H_2PO_4$ crystalline microparticles prepared with B-FDas (left), FDas (center), and FDry (right) with frozen spherical particles at concentrations of 0.02 g/g (first row), 0.06 g/g (second row), and 0.10 g/g (third row), respectively. The volume of the prepared frozen spherical particles was 0.04 cm^3. Scale bar: 10 μm.

Function of gas bubbles in freeze dissolving

With air bubbles during the whole dissolving process (0 min - 5 min), the $KHCO_3$ particles, shown in **Figure 9a**, are obviously smaller than the those obtained without air bubbles, shown in **Figure 9b**. The particles obtained with air bubbles at first half and second half process are shown in **Figure 9c** and **Figure 9d**. With air bubbles during the first half of the dissolving process (0 min - 2.5 min), the particles are like the products obtained without air bubbles, shown in **Figure 9A**. With air bubbles during the second half of the dissolving process (2.5 min - 5 min), the products obtained are like the products obtained with air bubbles during the whole process, shown in **Figure 9d**. The average sizes of these conditions are in the order, particles obtained without air bubbles > particles obtained with air bubbles during 0 min – 2. 5 min > particles obtained with air bubbles during 2.5 min – 5 min > particles obtained with air bubbles during 0 min – 5 min. Therefore, the air bubbles applied in both the first half dissolving process and second half dissolving have led to decrease in the particle size.

During the dissolving process, the presence of air bubbles in the solution led to the formation of smaller particles compared to conditions without bubbles. This size reduction is attributed to the cavitation effects generated by air bubbles, which enhance particle breakage and accelerate the dissolution rate [36]. The fragmentation of tiny ice parts from the larger frozen particles facilitates faster dissolution of both the fragments and the bulk frozen mass. Moreover, the dynamics of air bubbles, such as attachment, detachment, and collapse, could induce shake, rotation or other movements of the frozen particles [37,38]. These movements further would enhance mass transfer between the frozen particles and the surrounding solvent, contributing to an increased dissolution rate.

Although a similar duration of air bubble presence appears to have a consistent accelerating effect on dissolution, the results shown in Figure 9 reveal that air bubbles introduced during the later stage of dissolution have a more pronounced impact than those introduced at the initial stage. This suggests an additional mechanism. We propose that, beyond promoting ice dissolution, cavitation may also induce fragmentation of the product crystals, particularly in the case of needle-shaped particles. The addition of air bubbles lead to further decrease in the product crystal size in the later stage when most of the product crystals out of the frozen particles suspended in the solution. In contrast, during the initial stage, the effect was less not obvious due to the limited number of product crystals out of the frozen particles in the solution.

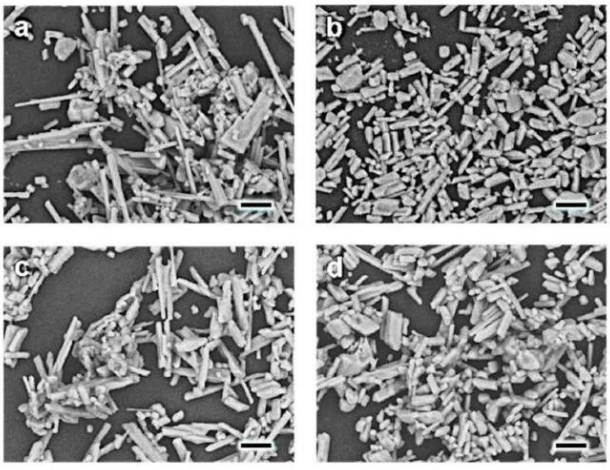

Figure 9. $KHCO_3$ particles obtained with (a) FDas (b) B-FDas of whole freeze-dissolving process with air bubbles for 0 min - 5 min, (c) with air bubbles only in 0 min - 2.5 min and (d) with air bubbles only in 2.5 min – 5 min. The concentration of the $KHCO_3$ solution used was 0.02 g/g, and the average volume of the frozen spherical particles was 0.06 cm^3. Scale bar: 10 μm.

View Article Online
DOI: 10.1039/D5NR01098E

ARTICLE

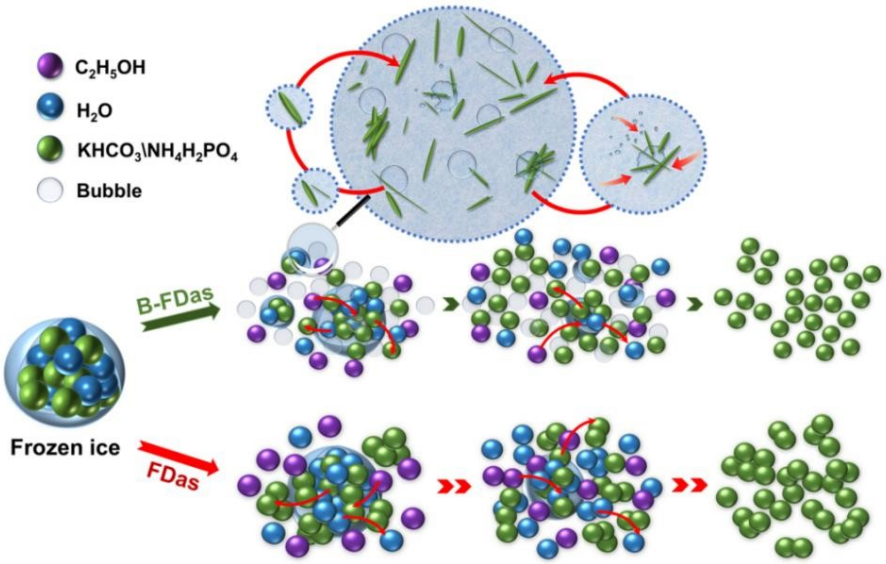

Figure 10. Proposed mechanisms of Freeze Dissolving with and without air bubbles.

Yield and energy consumption

The yield of B-FDas method is very high. For example, a 0.10 g/g $NH_4H_2PO_4$ solution was prepared, and 10 g of the solution was frozen in liquid nitrogen to form frozen ice particles. When these frozen particles were added in 70 g of ethanol at -20 °C, the ice parts in the frozen particles were dissolved in the ethanol. With dissolving of all the ice parts, the solution changed to water and ethanol mixture, with ratio of water and ethanol of about 1:7. At -20 °C, the solubility of $NH_4H_2PO_4$ in the mixture solution was very low, in the order of 10^{-3} g/g. With only about 1% of $NH_4H_2PO_4$ dissolved in the process, about 99% of $NH_4H_2PO_4$ remained in the solution, which could be collected after filtrations.

Figure 11 shows the energy consumption, estimated in the lab scale with consideration of relevant factors, including the entire process of liquid nitrogen production, transportation, and storage, as well as small particle preparation and ethanol recycling. Liquid nitrogen production relies on air separation technology, during transportation and storage, about 15% of the total energy is consumed due to heat transfer and evaporation. In this study, the first step for all three methods is same, forming frozen spherical particles by dripping $KHCO_3$ and $NH_4H_2PO_4$ solutions into liquid nitrogen. At a temperature of 295.15 K, approximately 60 g of liquid nitrogen was required to prepare 10 g of $KHCO_3$ solution. Approximately 30.8 kJ of energy is required to produce ice particles. However, the actual amount of liquid nitrogen needed in ideal conditions can be much less than the amount consumed during the experiment for unit weight of products.

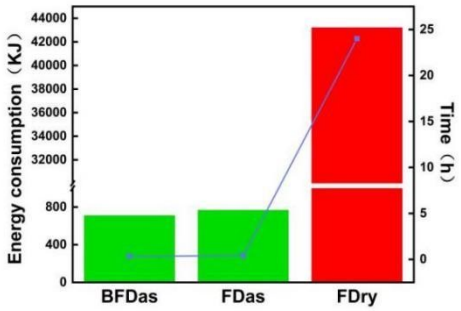

Figure 11. Comparison of energy and time consumption of three methods, B-FDas, FDas and FDry. The bar graph depicts energy consumption, and the line graph represents the time utilized.

The FDry method involved placing the frozen particles into a freeze-dryer, which required continuous operation of both a vacuum pump and a compressor under low-temperature vacuum conditions for 24 h. This setup resulted in substantial electricity consumption, with the vacuum pump operating at 400 W and the compressor at 100 W for a total duration of 1440 minutes. In contrast, the FDas and B-FDas methods followed a more energy-efficient three-step process: anti-solvent decomposition, filtration to separate the product, and drying. The FDas method required 15 minutes of operation for a water bath compressor at 200 W, 5 minutes

for a filtration pump at 200 W, and 5 minutes for a drying oven at 500 W. The B-FDas method, while incorporating an additional bubble air pump operating at 5 W for 10 minutes, significantly reduced the time required for the anti-solvent decomposition stage, further minimizing energy consumption. The energy consumption of recycling of ethanol and producing and transport of liquid nitrogen have been considered[39-41]. The liquid nitrogen can be produced via air separation technology, which are essential for all three technologies. The ethanol, used as an anti-solvent for only freeze dissolving technologies, can be recovered through distillation. A comparative calculation of energy consumption (supporting information of **Table S1**) reveals that the total energy consumption for FDry was 43,230.8 kJ, significantly higher than the 769.6 kJ consumed by FDas and the 712.6 kJ required by B-FDas. If the energy consumption for ethanol recovery is excluded, the energy consumption of B-FDas further drops to 363.8 kJ, accounting for less than 1% of that of FDry. These results highlight the energy-intensive nature of the FDry method compared to the more efficient FDas and B-FDas methods. Among them, the B-FDas method proved to be the most energy-efficient, attributed to its shorter processing times and the minimal energy requirements of the bubble generation unit. These findings demonstrate the potential of B-FDas a remarkably efficient and sustainable approach for fine particle preparation.

The B-FDas method demonstrates a sustainable and efficient approach for producing fine particles. For further scaling up, a large quantity of spherical ice particles will be produced in the first step. Spraying with a suitable nozzle will be required to control the droplet size during injection into liquid nitrogen. It would be valuable to explore the applicability of this technology to other systems, such as in the fields of medicine and catalysis, where the production of particles at the nanometer scale is often required [42-45]. To apply this technology for producing nano particles of target chemicals, including inorganic and organic compounds [46,47], two compatible solvents are required. One solvent has high solubility for the target product, and it should have a relatively high freezing point. The other one is anti-solvent with low solubility for the target product and a lower freezing point than the first solvent. The process involves freezing the solution of the target chemicals in the first solvent to form frozen particles. Then the frozen particles are dissolved into anti-solvent at a controlled temperature between the freezing points of the first solvent and the anti-solvent. The frozen parts (frozen of first solvent) in the frozen particles can be dissolve, and the nanosized product to remain dispersed in the anti-solvent.

In summary, this study introduces a novel B-FDas method for micro-particle preparation, which demonstrates significant advantages over the conventional FDry method. The B-FDas method not only produces smaller particles and less agglomeration but also exhibits remarkably lower energy consumption and faster processing speed. Its applicability to both inorganic and organic compounds highlight its potential for widespread use in the preparation of micro and nano particles. The insights gained from this research pave the way for more efficient and sustainable particle production technologies. Other technologies for enhancing the mass transfer, such as ultrasounds and wet milling could be further explored.

Conclusions

In this study, we developed an innovative technique with air bubbles during the freeze-dissolving (B-FDas) process to prepare fine particles. Compared with Freeze-drying (FDry) method, the particles obtained with B-FDas have smaller size and lighter agglomeration. The trend is consistent in both two systems $KHCO_3$ and $NH_4H_2PO_4$, with frozen particles from 0.01 to 0.08 cm^3 and with solution concentration from 0.02 g/g to 0.10 g/g. The smaller microparticles are both obtained with low solution concentration and smaller frozen particles volume with B-FDas method. The smallest microparticles of $KHCO_3$ and $NH_4H_2PO_4$ obtained by B-FDas method are 10.20 ± 0.63 µm and 13.67 ± 0.73 µm, respectively. The particles obtained by FDas are bigger, and the particles obtained by FDry are largest at equal condition. All the fine particles show good crystalline structure, but the shape of particles by B-FDas are usually more regular. The energy consumption of B-FDas is merely less than 1% of that of FDry, yet its processing speed is 100 times faster than that of FDry.

Author contributions

Qiutong Zhang: Data curation, Visualization, Writing -original draft, Writing - review & editing, Investigation, Validation, Methodology, Software.
Jiaqi Luo: Supervision, Methodology. **Yingchen Wang:** Methodology. **Wenhao Yan:** Software. **Yimin Jia:** Investigation.
Mingting Yuan: Formal analysis. **Yuan Zou:** Formal analysis. **Xinyue Zhai:** Investigation. **Qiushuo Yu:** Methodology, Project administration, Resources, Conceptualization, Funding acquisition, Supervision. **Huaiyu Yang:** Methodology, Conceptualization, Writing - review & editing, Project administration, Supervision.
The manuscript was written through contributions of all authors. All authors have given approval to the final version of the manuscript.

Conflicts of interest

There are no conflicts to declare.

Data availability

The data associated with this article, including an Excel spreadsheet containing particle size distribution data, are available at Mendeley Data. The dataset can be accessed via the following link: https://data.mendeley.com/preview/yg3fmrfdb7?a=d2c40398-c3e5-480c-8122-bfeb5ed4b906.

View Article Online
DOI: 10.1039/D5NR01690E

Acknowledgements

The authors are grateful to the National Science Foundation (NSFC21978234) for financial assistance in this project.

References

1 N. Ichinose, Y. Ozaki, S. Kashū, Fundamentals of Superfine Particles, in: Superfine Particle Technology, Springer London, London, 1992: pp. 1–19. https://doi.org/10.1007/978-1-4471- 1808-4_1.
2 L. Wang, H. Ji, S. Wang, L. Kong, X. Jiang, G. Yang, Preparation of Fe3O4 with high specific surface area and improved capacitance as a supercapacitor, Nanoscale 5 (2013) 3793. https://doi.org/10.1039/c3nr00256j.
3 O.G. Apul, N. Hoogesteijn von Reitzenstein, J. Schoepf, D. Ladner, K.D. Hristovski, P. Westerhoff, Superfine powdered activated carbon incorporated into electrospun polystyrene fibers preserve adsorption capacity, Science of The Total Environment 592 (2017) 458–464. https://doi.org/10.1016/j.scitotenv.2017.03.126.
4 D. Vollath, F.D. Fischer, D. Holec, Surface energy of nanoparticles – influence of particle size and structure, Beilstein Journal of Nanotechnology 9 (2018) 2265–2276. https://doi.org/10.3762/bjnano.9.211.
5 M.A. Ibrahim, M.Z. Jaafar, M.A.M. Yusof, C.A. Shye, A.K. Idris, Influence of size and surface charge on the adsorption behaviour of silicon dioxide nanoparticles on sand particles, Colloids Surf A Physicochem Eng Asp 674 (2023) 131943. https://doi.org/10.1016/j.colsurfa.2023.131943.
6 R.A. Arnold, I.L. Motta, J.M. Hill, Impact of particle size and catalyst dispersion on gasification rates measured in a thermogravimetric analysis unit: Case study of carbon black catalyzed by potassium or calcium, Fuel 288 (2021) 119677. https://doi.org/10.1016/j.fuel.2020.119677.
7 S. Cao, F. (Feng) Tao, Y. Tang, Y. Li, J. Yu, Size- and shape-dependent catalytic performances of oxidation and reduction reactions on nanocatalysts, Chem Soc Rev 45 (2016) 4747–4765. https://doi.org/10.1039/C6CS00094K.
8 N. Hoshyar, S. Gray, H. Han, G. Bao, The Effect of Nanoparticle Size on In Vivo Pharmacokinetics and Cellular Interaction, Nanomedicine 11 (2016) 673–692. https://doi.org/10.2217/nnm.16.5.
9 B.J. Abdullah, Size effect of band gap in semiconductor nanocrystals and nanostructures from density functional theory within HSE06, Mater Sci Semicond Process 137 (2022) 106214. https://doi.org/10.1016/j.mssp.2021.106214.
10 T. Gomathi, K. Rajeshwari, V. Kanchana, P.N. Sudha, K. Parthasarathy, Impact of nanoparticle shape, size, and properties of the sustainable nanocomposites, in: Sustainable Polymer Composites and Nanocomposites, Springer International Publishing, 2019: pp. 313–336. https://doi.org/10.1007/978-3-030-05399-4_11.
11 S. Jeon, W. Jung, H. Bae, S. Ahn, B. Koo, W. Yu, S. Kim, D. Oh, U. Kim, S.A. Barnett, J. Seo, B. Kim, W. Jung, Concurrent Amorphization and Nanocatalyst Formation in Cu-Substituted Perovskite Oxide Surface: Effects on Oxygen Reduction Reaction at Elevated Temperatures, Advanced Materials (2024). https://doi.org/10.1002/adma.202404103.
12 S. Sun, H. Li, Z.J. Xu, Impact of Surface Area in Evaluation of Catalyst Activity, Joule 2 (2018) 1024–1027. https://doi.org/10.1016/j.joule.2018.05.003.
13 S. Shan, J. Li, Y. Maswadeh, C. O'Brien, H. Kareem, D.T. Tran, I.C. Lee, Z.-P. Wu, S. Wang, S. Yan, H. Cronk, D. Mott, L. Yang, J. Luo, V. Petkov, C.-J. Zhong, Surface oxygenation of multicomponent nanoparticles toward active and stable oxidation catalysts, Nat Commun 11 (2020) 4201. https://doi.org/10.1038/s41467-020-18017-3.
14 Y. Wang, Z. Zhang, Z. Yin, J. Wang, X. Zhang, C. Chen, Adsorption of typical NDMA precursors by superfine powdered activated carbon: Critical role of particle size reduction, Journal of Environmental Sciences 147 (2025) 101–113. https://doi.org/10.1016/j.jes.2023.10.016.
15 B. Sonmez Baghirzade, P. Biswas, S. Moavenzadeh Ghaznavi, B. Frederick, J.F. Reuther, O.G. Apul, Accessibility of adsorption sites for superfine powdered activated carbons incorporated into electrospun polystyrene fibers, Chemical Engineering Journal 461 (2023) 142009. https://doi.org/10.1016/j.cej.2023.142009.
16 J. Zhang, L. Liu, C. Zheng, W. Li, C. Wang, T. Wang, Embedded nano spin sensor for in situ probing of gas adsorption inside porous organic frameworks, Nat Commun 14 (2023) 4922. https://doi.org/10.1038/s41467-023-40683-2.
17 T.T. Truong, S. Mondal, V.H.M. Doan, S. Tak, J. Choi, H. Oh, T.D. Nguyen, M. Misra, B. Lee, J. Oh, Precision-engineered metal and metal-oxide nanoparticles for biomedical imaging and healthcare applications, Adv Colloid Interface Sci 332 (2024) 103263. https://doi.org/10.1016/j.cis.2024.103263.
18 X. Han, K. Xu, O. Taratula, K. Farsad, Applications of nanoparticles in biomedical imaging, Nanoscale 11 (2019) 799–819. https://doi.org/10.1039/C8NR07769J.
19 A. Campos, N. Troc, E. Cottancin, M. Pellarin, H.-C. Weissker, J. Lermé, M. Kociak, M. Hillenkamp, Plasmonic quantum size effects in silver nanoparticles are dominated by interfaces and local environments, Nat Phys 15 (2019) 275–280. https://doi.org/10.1038/s41567-018-0345-z.
20 Y. Volokitin, J. Sinzig, L.J. de Jongh, G. Schmid, M.N. Vargaftik, I.I. Moiseevi, Quantum-size effects in the thermodynamic properties of metallic nanoparticles, Nature 384 (1996) 621–623. https://doi.org/10.1038/384621a0.
21 N. Joshi, N. Mathur, T. Mane, D. Sundaram, Size effect on melting temperatures of alumina nanocrystals: Molecular dynamics simulations and thermodynamic modeling, Comput Mater Sci 145 (2018) 140–153. https://doi.org/10.1016/j.commatsci.2017.12.064.
22 Z. Hongya, et al., "Research on the preparation of superfine ammonium dihydrogen phosphate by new processes", Nanjing University of Science and Technology, 2009. DOI: 10.7666/d. y1541787.
23 J. Zhao, et al., Insights into the particle diameter and base chosen for dry powder fire extinguishing agents, Fire and Materials. DOI: 10.1002/fam.3117.
24 Q. Yu, Y. Wang, J. Luo, H. Yang, Freeze-Dissolving Method: A Fast Green Technology for Producing Nanoparticles and Ultrafine Powder, ACS Sustain Chem Eng 10 (2022) 7825–7832. https://doi.org/10.1021/acssuschemeng.2c02270.
25 J. Luo, Q. Su, Q. Yu, X. Zhai, Y. Zou, H. Yang, Application of efficient and sustainable freeze-dissolving technology in manufacturing of KHCO3 ultrafine particles, Green Chemical Engineering 5 (2024) 266–272. https://doi.org/10.1016/j.gce.2023.07.003.
26 J. Luo, Q. Su, Q. Yu, X. Zhai, Y. Zou, H. Yang, Fast and simple preparation of microparticles of $KHCO_3$ by a freeze-dissolving method with single solvent or additional antisolvent, RSC Sustainability 1 (2023) 1982–1988. https://doi.org/10.1039/D3SU00234A.
27 Kotake, N.; Kuboki, M.; Kiya, S.; Kanda, Y. Influence of Dry and Wet Grinding Conditions on Fineness and Shape of Particle Size Distribution of Product in a Ball Mill. Advanced

Powder Technology 2011, 22 (1), 86 – 92. https://doi.org/10.1016/j.apt.2010.03.015.
28 Wei, L.; Abd Rahim, S.; Al Bakri Abdullah, M.; Yin, A.; Ghazali, M.; Omar, M.; Nemeș, O.; Sandu, A.; Vizureanu, P.; Abdellah, A. Producing Metal Powder from Machining Chips Using Ball Milling Process: A Review. Materials 2023, 16 (13), 4635. https://doi.org/10.3390/ma16134635.
29 Alavizadeh, S. A. R.; Shahbaz, M.; Kavanlouei, M.; Kim, S. S. The Effect of Mechanical Milling for Enhanced Recycling Ti6Al4V Powder from Machining Chips. Sci Rep 2025, 15 (1), 444. https://doi.org/10.1038/s41598-024-84913-z.
30 Bagheri, N.; Nosratinia, F.; Zahakifar, F.; Yousefi, T. The Effect of Operational Parameters on the Properties of Thorium Uranium Oxide Produced via Oxalates ' Coprecipitation. Sci Rep 2025, 15 (1), 18536. https://doi.org/10.1038/s41598-025-03675-4.
31 Farahani, B. V.; Rajabi, F. H.; Bahmani, M.; Ghelichkhani, M.; Sahebdelfar, S. Influence of Precipitation Conditions on Precursor Particle Size Distribution and Activity of Cu/ZnO Methanol Synthesis Catalyst. Appl Catal A Gen 2014, 482, 237 – 244. https://doi.org/10.1016/j.apcata.2014.05.034.
32 Nason, J. A.; Lawler, D. F. Particle Size Distribution Dynamics during Precipitative Softening: Declining Solution Composition. Water Res 2009, 43 (2), 303 – 312. https://doi.org/10.1016/j.watres.2008.10.017.
33 Valverde Aguilar, G. Introductory Chapter: A Brief Semblance of the Sol-Gel Method in Research. In Sol-Gel Method - Design and Synthesis of New Materials with Interesting Physical, Chemical and Biological Properties; IntechOpen, 2019. https://doi.org/10.5772/intechopen.82487.
34 Navas, D.; Fuentes, S.; Castro-Alvarez, A.; Chavez-Angel, E. Review on Sol-Gel Synthesis of Perovskite and Oxide Nanomaterials. Gels 2021, 7 (4), 275. https://doi.org/10.3390/gels7040275.
35 Bokov, D.; Turki Jalil, A.; Chupradit, S.; Suksatan, W.; Javed Ansari, M.; Shewael, I. H.; Valiev, G. H.; Kianfar, E. Nanomaterial by Sol – Gel Method: Synthesis and Application. Advances in Materials Science and Engineering 2021, 2021 (1). https://doi.org/10.1155/2021/5102014.
36 E. V. Skorb, H. Möhwald, D. V. Andreeva, Effect of Cavitation Bubble Collapse on the Modification of Solids: Crystallization Aspects, Langmuir 32 (2016) 11072–11085. https://doi.org/10.1021/acs.langmuir.6b02842.
37 E. Loth. Quasi-steady shape and drag of deformable bubbles and drops. International Journal of Multiphase Flow. 34 (2008) 523-546. https://doi.org/10.1016/j.ijmultiphaseflow.2007.08.010.
38 X. Xu, J. Zhang, F. Liu, X. Wang, W. Wei, Z. Liu. Rising behavior of single bubble in infinite stagnant non-Newtonian liquids. International Journal of Multiphase Flow. 95 (2017) 84-90. DOI: 10.1016/j.ijmultiphaseflow.2017.05.009.
39 Rizvi, S. F. J., Miran, S., Azam, M., Arif, W., Wasif, M., & Garcia, H. P. (2021). Numerical Analysis of a Liquid Nitrogen (LN2) Engine for Efficient Energy Conversion. ACS Omega.https://doi.org/10.1021/acsomega.1c00582
40 How on-site nitrogen generation reduces your operating costs. Accessed September 4, 2023. Available. at: https://maziak.co.uk/news-and-media/how-on-site-nitrogen-generation-reduces-your-operating-costs?__cf_chl_rt_tk=7KYLpfjYpi7oZPW8mxGYV201G.TEl8xf9Bm4otgMYWk-1693807407-0-gaNycGzNDWU
41 Guo, Y., Chen, S., Ma, S., & Liu, C. (2017). Optimization of aqueous ethanol distillation based on Aspen simulation. Chemical Industry and Engineering Progress, 36 (Suppl. 1), 80–86. https://doi.org/10.16085/j.issn.1000-6613.2016-2438
42 H. Tonbul, A. Sahin, E. Tavukcuoglu, G. Esendagli, Y. Capan. Combination drug delivery with actively-targeted PLGA nanoparticles to overcome multidrug resistance in breast cancer. Journal of Drug Delivery Science and Technology. 54(2019) 101380, https://doi.org/10.1016/j.jddst.2019.101380.
43 M. Cheraghi, B. Negahdari, H. Daraee, A. Eatemadi. Heart targeted nanoliposomal/nanoparticles drug delivery: An updated review. Biomedicine & Pharmacotherapy. 86(2017) 316-323. https://doi.org/10.1016/j.biopha.2016.12.009.
44 Yazan Mahayni, Lukas Maurer, Franziska Auer, Andreas Hutzler, Peter Wasserscheid, Moritz Wolf. Structure sensitivity of the low-temperature dehydrogenation of perhydro dibenzyltoluene on supported platinum nanoparticles. Catalysis Science & Technology. 2024,14, 5464-5473. DOI: https://doi.org/10.1039/D4CY00032C.
45 .Gonzalo Prieto, Harun Tüysüz, Nicolas Duyckaerts, Johannes Knossalla, Guang-Hui Wang, Ferdi Schüth. Hollow Nano- and Microstructures as Catalysts. Chemical Reviews. 2016, 116, 22, 14056–14119. https://doi.org/10.1021/acs.chemrev.6b00374.
46 J. Luo, Y. Wang, Q. Su, Q. Yu, X. Zhai, Y. Zou, Q. Zhang, W. Yan, H. Yang. Rapid and sustainable production of nano and micro medicine crystals via freeze-dissolving technology. Powder Technology. 443 (2024) 2753-2765, DOI: 10.1016/j.powtec.2024.119913.
47 C. Guo, Y. Wang, Q. Su, X. Zhai, Y. Zou, Q. Zhang, W. Yan, H. Yang. A Scalable Freeze-Dissolving Approach to Prepare Ultrafine Crystals for Inhalation: Mechanism and Validation. Crystal Growth & Design. 24 (2024) 2918-2931. DOI: 10.1021/acs.cgd.4c00018.

View Article Online
DOI: 10.1039/D5NR01098E

Data Availability Statement

The data associated with the article titled "Efficient and sustainable preparation of ultrafine particles by bubble-assisted freeze-dissolving method" are available on the Mendeley Data platform. The dataset includes two Excel spreadsheets: containing detailed particle size distribution data. These spreadsheets are essential for understanding the results and methodology of this study. The dataset can be accessed via the following link: https://data.mendeley.com/preview/yg3fmrfdb7?a=d2c40398-c3e5-480c-8122-bfeb5ed4b906.

The data are intended for academic research purposes only and are not to be used for commercial or other non-academic purposes. Users are required to acknowledge the original source and authors when using or referencing the data.

For further information or assistance with data access, please contact the corresponding author at *H.yang3@lboro.ac.uk* or visit the Mendeley Data support page.